Proceedings of the 17th World Congress
The International Federation of Automatic Control
Seoul, Korea, July 6-11, 2008

CONTROL OF A FLEXIBLE ROBOT USING FUZZY LOGIC AND A NONCOLLOCATED SENSOR

A. Green J. Z. Sasiadek

Department of Mechanical and Aerospace Engineering,
Carleton University, Ottawa, Ontario, K1S 5B6.

Abstract: Inverse flexible dynamics control (IFDC) and fuzzy logic system adaptive control (FLSAC) strategies are used to track the end effector of a flexible space robot with sensors collocated at the joints, noncollocated at the end effector and 0.5m from the elbow joint on link 2. Collocated joint sensors satisfy hyperstability conditions but fail to capture nonminimum phase (NMP) response that generates time-delays causing asynchronous control action. Noncollocated sensors capture NMP response but require time delay compensation to achieve synchronous control action. Results for IFDC are insignificant compared to those achieved with FLSAC.

Keywords: Flexible Robot, Sensor Location, Fuzzy Control, Nonminimum Phase

1. INTRODUCTION

Long slender flexible multibody space robot manipulators present great difficulty in tracking control during spacecraft operations. Ideally a sensor located at the end effector captures true position data but presents NMP response time-delayed feedback signals. Precise control requires either synchronization of control action to compensate for time-delayed feedback signals or suppression of the flexible link vibrations. IFDC and FLSAC strategies with NMP time delays and time-delayed control action are compared in the control of a two-link flexible robot with collocated and noncollocated sensors tracking a 12.6m x 12.6m square trajectory with the shoulder joint at its centre. Abrupt orthogonal direction switches generate large amplitude transient flexural vibrations to demonstrate the effect of both strategies.

The contribution in this paper is shown by the significant reduction in vibration and NMP response and greater tracking control precision achieved using a FLSAC strategy for a sensor located at the end effector and 0.5m from the elbow joint on link 2 where the influence of link 1 endpoint vibration is severe. In comparison the use of an IFDC strategy with time-delayed control action only to compensate for NMP response is ineffective.

Green and Sasiadek (2005a) use a fuzzy logic system (FLS) to adapt the control law for a flexible robot. Green and Sasiadek (2005b) compare IFDC and FLSAC control strategies with NMP time delay and synchronized control action for sensors located at the end effector and 2.25m from the end effector of a two-link flexible robot. Results show stable trajectories for both strategies but a significant reduction in vibration amplitude and NMP response is achieved with FLSAC. Stieber et al (1997) propose an extended hyperstability control concept for a flexible robot with conventional hyperstable control sensors used in conjunction with performance sensors to enable vision-based stable control of large flexible space robot manipulators,. The strategy effectively overcomes the restrictions of conventional hyperstable control. Liang and Balas use a reduced-order model and Popov's hyperstability theory to represent large space structures (LSS) with four vibration modes. Direct MRAC simulation results for a single-link flexible robot manipulator with angular displacement sensors located at the hub, midlink and the endpoint show excellent model following, flexibility in choice of adaptive laws and avoidance of difficulties in using Lyapunov's stability function. Karkoub et al (1995) perform theoretical and experimental studies on a single-link flexible manipulator using the μ-synthesis control method. Feedback control experiments use a collocated hub angle sensor, hub angle and endpoint acceleration sensors, and hub and endpoint sensors for which the hub angle specification is relaxed to reduce hub response overshoot. Results validate the two theoretical noncollocated sensor designs as dramatically improving control and robustness over the collocated hub angle sensor. Ryan, Kwon and Hannaford (2004) propose a time-domain passivity-control approach to a single-link flexible manipulator with noncollocated sensor feedback. Simulation results show time-domain passivity-control to be effective for both large and small tip displacements.

Nonminimum phase response is an inherent problem with flexible robot control. The phenomenon occurs when torque actuates a robot joint, induces flexure and momentary acceleration of the end effector in a direction opposite in sense to that commanded with time-delayed position feedback causing asynchronous control action. The delay is the length of time for a mechanical wave to propagate through the link from joint to end effector. In analytical control theory this behaviour occurs when transfer function zeros exist in the right half s-plane and termed a phase shift or, transport lag, between the actuator and end effector. The zero-dynamics must be asymptotically stable for a minimum-phase system with transfer function zeros occurring in the left half plane. Otherwise, NMP response occurs and may become unstable. Hence, some form of zero-dynamics control is required to stabilize the system. Control strategies including; integral manifolds, input-output decoupling, observer-based decoupling and inverse dynamics sliding mode have resulted in robust closed-loop performance and reduced end-effector position tracking errors, but at increased control system complexity and computational time unsuitable for real-time applications, Slotine and Li (1991). Associated with NMP response is the distance between sensor and actuator. Noncollocated sensors are located at some position on the robot links to measure its position. Collocated sensors are mounted at robot joints to measure rotation angle displacements and are more suited for fixed-base rigid-link robots operating at speeds where flexibility is insignificant. Flexible robots exhibit significant deformation at the end effector necessitating accurate control by adjusting for phase shift between actuator and end effector, Alexander (1988). When a sensor is collocated with a joint actuator on a flexible robot it is a *hyperstable* system. Hyperstable systems require; sensors and actuators equal in number, matching types of sensors and actuators and sensor/actuator collocation, (Stieber et al 1997, Liang and Balas 1990). But, these conditions detract from proper control of flexible robots. The flexible robot dynamics in (6) and (7) for the dominant mode of vibration and a noncollocated sensor are considered stable by the Routh-Hurwitz criterion, Stieber et al (1997).

2. FLEXIBLE ROBOT

The flexible robot shown in Fig. 1 has planar motion and vibration modes. Gravity and friction are omitted. Lengths of each flexible link $L_1 = L_2 = 4.5$m; flexural rigidity EI = 1676 N-m^2 and link mass density $\rho = 0.335$ kg/m.

Flexible Dynamics

Closed-form Euler-Lagrange flexible dynamics equations model the robot in terms of its kinetic and potential energies and include link flexibility based on the dominant assumed mode for an Euler-Bernoulli cantilever beam coupled with rotating rigid-link dynamics. Given an independent set of generalized coordinates, $\mathbf{q} = q_1, q_2$, the total kinetic energy T and potential energy U of the system is defined by the Lagrangian (De Luca and Siciliano 1991):

$$\mathfrak{L}\left(q_i, \dot{q}_i\right) = T - U, \qquad i = 1, 2 \tag{1}$$

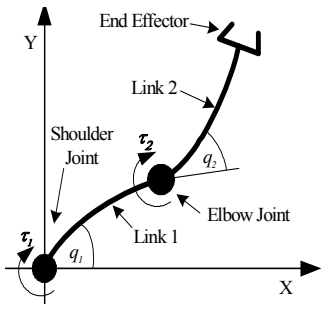

Fig. 1. Flexible robot.

When a generalized force vector **F** acts on generalized coordinates **q** the dynamic equations of motion are given by:

$$\frac{d}{dt}\frac{\partial \mathfrak{L}}{\partial \dot{\mathbf{q}}} - \frac{\partial \mathfrak{L}}{\partial \mathbf{q}} = \mathbf{F} \tag{2}$$

Achieving accurate tracking control of a two-link robot is compounded by distributed flexibility of its links, flexural vibrations and NMP response. For precision control the residual vibrations must be suppressed while compensating for NMP response (Moallem et al 2000, Slotine and Li 1991). Assumed modal expansions are used in the derivation of the Euler-Lagrange equations to model each link as an Euler-Bernoulli cantilever beam. Assumed modes accommodate changes in configuration during operation, whereas natural modes must be continually recomputed. Elastic deformations of the robot links are modeled by a finite series of space-dependent, *admissible functions,* multiplied by a specific set of time-dependent amplitude functions, resulting in a deformation function. A chosen set of admissible functions should satisfy, at least, the flexible robot geometric boundary conditions and form basis functions applying throughout its operational workspace, provided the boundary conditions are consistent. An approximate deformation of the robot links subjected to transverse vibrations is given by, Thomson (1981):

$$u(x, t) = \sum_{i=1}^{n} \varphi_i(x) q_i(t) \tag{3}$$

where**;** $\varphi_i(x)$ are assumed mode shapes.
From transverse beam vibration theory, cantilever mode shapes are given by:

$$\varphi_{ci}(x) = A\left[\cosh\lambda_{ci}x - \cos\lambda_{ci}x - k_{ci}\left(\sinh\lambda_{ci}x - \sin\lambda_{ci}x\right)\right] \tag{4}$$

where; $A = 0.1$ is an arbitrary constant, $\lambda_{ci}L = (i - 0.5)\pi$, $i = 1,\ldots\ldots,n$ are numerically approximated roots of the characteristic equation $\cos(\lambda_{ci}L)\cosh(\lambda_{ci}L) + 1 = 0$ and $k_{ci} = \cos\lambda_{ci}L + \cosh\lambda_{ci}L \,/\, \sin\lambda_{ci}L + \sinh\lambda_{ci}L$.
Modal frequencies are given by:

$$\omega_{ci} = (\lambda_{ci}L)^2\sqrt{EI/\rho L^4} \quad (5)$$

Using the deformation function u(x, t) given in (3) for an Euler-Bernoulli cantilever beam the Euler-Lagrange flexible robot dynamics matrix equations are given by:

$$\boldsymbol{\tau} = \mathbf{M}(\mathbf{q})\ddot{\mathbf{q}} + \mathbf{C}(\mathbf{q},\dot{\mathbf{q}}) + \mathbf{K}\mathbf{q} \quad (6)$$

M is a matrix of rigid and flexible-link inertia elements, **C** is a matrix of rigid Coriolis and centrifugal forces, **K** is a stiffness matrix and **q** is a generalized coordinate vector of joint angles and elastic deformations. Because of the orthogonality properties of assumed modes second-order terms of interacting elastic modes can be neglected and elastic components may be omitted in $\mathbf{C}(\mathbf{q},\dot{\mathbf{q}})$ that simplifies to $\mathbf{C}_r(\boldsymbol{\theta},\dot{\boldsymbol{\theta}})$ for rigid dynamics. Alternatively, (6) may be expressed as:

$$\begin{bmatrix}\boldsymbol{\tau}\\ \mathbf{0}\end{bmatrix} = \mathbf{M}(\boldsymbol{\theta},\boldsymbol{\delta})\begin{bmatrix}\ddot{\boldsymbol{\theta}}\\ \ddot{\boldsymbol{\delta}}\end{bmatrix} + \begin{bmatrix}\mathbf{C}_r(\boldsymbol{\theta},\dot{\boldsymbol{\theta}})\\ \mathbf{0}\end{bmatrix} + \begin{bmatrix}\mathbf{0} & \mathbf{0}\\ \mathbf{0} & \mathbf{K}\end{bmatrix}\begin{bmatrix}\boldsymbol{\theta}\\ \boldsymbol{\delta}\end{bmatrix} \quad (7)$$

Where; the zero-dynamics are system internal dynamics for which the input and output of the system is identically zero. The internal dynamics of the flexible robot include elastic deformations of the links δ_i, Moallem et al (2000).

3. CONTROL STRATEGIES

Inverse flexible dynamics control (IFDC)

The IFDC strategy is shown in Fig. 3. Torque feeds into the flexible dynamics equations and actuates each robot joint for acceleration output. Slew angles θ_1 and θ_2 and flexural deformations δ_i, i = 1, 2, feed back into the flexible dynamics equations and θ_1 and θ_2 also transform into x and y end effector positions in (8) and (9). Slew angles θ_1 and θ_2 and slew rates $\dot{\theta}_1$, $\dot{\theta}_2$ feed back to form position errors $\mathbf{e}_x$ and $\mathbf{e}_y$, and velocity errors $\dot{\mathbf{e}}_x$ and $\dot{\mathbf{e}}_y$. Rigid-link robot kinematics equations relating end-effector positions x and y to joint angles θ_1 and θ_2 are given by:

$$x = L_1\cos(\theta_1) + L_2\cos(\theta_1+\theta_2) \quad (8)$$

$$y = L_1\sin(\theta_1) + L_2\sin(\theta_1+\theta_2) \quad (9)$$

Position and velocity errors are multiplied by proportional and derivative (PD) gains, $\mathbf{K_p}$ and $\mathbf{K_d}$ to compute a Jacobian transpose control law given by.

$$\boldsymbol{\tau} = \mathbf{J}^T(\boldsymbol{\theta})\left[\mathbf{K}_p\begin{pmatrix}\mathbf{e}_x\\ \mathbf{e}_y\end{pmatrix} + \mathbf{K}_d\begin{pmatrix}\dot{\mathbf{e}}_x\\ \dot{\mathbf{e}}_y\end{pmatrix}\right] \quad (10)$$

Proportional and derivative gains for the dominant cantilever assumed mode frequency ω_{c1} are given by.

$$\mathbf{K_p} = \mathrm{diag}\left[\omega_{c1}^2 \quad \omega_{c1}^2\right] = \mathrm{diag}\left[150.79, 150.79\right] \quad (11)$$

$$\mathbf{K_d} = \mathrm{diag}\left[2\zeta\omega_{c1} \quad 2\zeta\omega_{c1}\right] = \mathrm{diag}\left[17.364, 17.364\right] \quad (12)$$

Where, ω_{c1} = 12.28 Hz and damping ratio ζ = 0.707. Using (8) and (9) the Jacobian **J** is derived as:

$$\mathbf{J} = \begin{bmatrix}\frac{\partial x}{\partial\theta_1} & \frac{\partial x}{\partial\theta_2}\\ \frac{\partial y}{\partial\theta_1} & \frac{\partial y}{\partial\theta_2}\end{bmatrix} = \begin{bmatrix}-L_1\sin\theta_1 - L_2\sin(\theta_1+\theta_2) & -L_2\sin(\theta_1+\theta_2)\\ L_1\sin\theta_1 + L_2\cos(\theta_1+\theta_2) & L_2\cos(\theta_1+\theta_2)\end{bmatrix} \quad (13)$$

Fuzzy logic system adaptive control (FLSAC)

The Mamdani FLS shown in Fig. 4 is developed intuitively with three membership functions (MF), i.e. 9 rules for input and output variables shown in Fig. 2 (a) and (b).

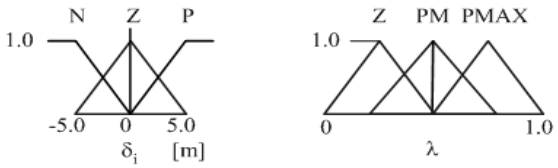

(a) (b)

Fig. 2. Fuzzy membership functions: (a) δ_i, i = 1, 2, (b) Output variableλ.

Universes of discourse range from -5m to 5m for δ_1 and δ_2 and from 0 to 1 for λ. Verbal descriptors for positive maximum (PMAX), positive very very high (PVVH), positive very high PVH), positive high (PH), positive medium (PM), positive low (PL), positive very low (PVL), positive very very low (PVVL), positive (P), zero (ZERO), negative very high (NVH), negative high (NH), negative medium (NM), negative low (NL), negative very low (NVL) and negative (N) are used to generate fuzzy rules typically of the form. 'IF δ_1 is NL AND δ_2 is PL THEN λ is PM'. The FLS uses antecedent composition (MIN), implication (MIN), aggregation (MAX) and defuzzification (CENTROID). Elastic link deformations δ_1 and δ_2 vary positively or negatively and either complement or counter deformation of the other link to produce a resultant deformation within a range from ZERO for zero deformation to PMAX for the largest deformation.

Table 1 Fuzzy logic system rule matrix for three triangular membership functions (9 rules).

		δ_2		
	λ	N	ZERO	P
δ_1	N	PMAX	PM	PMAX
	ZERO	PM	ZERO	PM
	P	PMAX	PM	PMAX

These link interactions enable formation of the symmetric fuzzy rule matrix given in Table 1.

The value of λ is determined by the fuzzy rules according to the values of δ_1 and δ_2 whose MF base widths are adjusted by K_s to adapt the Jacobian transpose control law. For example, as link 1 rotates it experiences acceleration and deceleration, interacts with link 2 and excites vibration and variation of δ_1 through N, ZERO and P. Link 2 rotates and also excites vibration and variation of δ_2 through N, ZERO and P. The fuzzy rule matrix in Table 1 is designed such that when δ_1 and δ_2 fall into either P or N the value of λ is always PMAX, i.e. $\lambda = 1$, and adapts the control law to the maximum for each joint. Fuzzy rules with either δ_1 or δ_2 being ZERO produce a value of $\lambda < 1$, i.e. PM, to adapt the control law by a value between ZERO and PMAX for each joint actuator. For both δ_1 and δ_2 at ZERO the control law adaptation is minimal or zero. Values of δ_1 and δ_2 are normalized by gain $K_n = 5$ before entering the FLS [2].

The adaptive form of $\boldsymbol{\tau}_r$ in (14) is given by [2].

$$\boldsymbol{\tau}_r = K_S\lambda\left\{\mathbf{J}^T(\boldsymbol{\theta})\left[\mathbf{K}_p\begin{pmatrix}e_x\\e_y\end{pmatrix}+\mathbf{K}_d\begin{pmatrix}\dot{e}_x\\\dot{e}_y\end{pmatrix}\right]\right\} \tag{14}$$

The control strategy shown in Figs. 3 and 4 is used to demonstrate control with a noncollocated sensor as joint angles and rates are transformed into end-effector positions and velocities for control law computation. Time delays are implemented in the feedback loop to model the effect of NMP because there is no provision for traveling wave velocity and associated time delays in the robot dynamics equations and the system output variables are joint rotation angles and link deformations. Therefore, it is necessary to model sensors located at points on the links by including direct kinematics equations with link lengths, L_1 and L_2, as the distance between joint and sensor to feedback x and y coordinate measurements of the sensor. Direct kinematics equations for the end effector are also included to track the end effector trajectory. Transport delay blocks (not shown) are implemented in Matlab/Simulink™ models. NMP response is corrected by time delays for command signals input to the control law. Time delays are calculated using the transverse beam vibration traveling wave velocity c given by.

$$c = \sqrt{\frac{E}{\rho}} = \sqrt{\frac{1745833}{21}} = 288.33 \text{ m/s} \tag{15}$$

Delay time from joint 1 to end effector for two link lengths, i.e. 9m, is given by:

$$t_{d_1} = \frac{9}{288.33} = 0.0312\text{s} \tag{16}$$

Average trajectory simulation time is 402s for 16000 simulation steps (ss) at 0.001step size, i.e. 0.0252s per step.

$\therefore$ Simulation delay time from joint 1 to end effector:

$$d_1 = \frac{0.0312}{0.0252} = 1.238\text{ss} \tag{17}$$

Delay time from joint 2 to end effector for one link length of 4.5m is given by:

$$t_{d_2} = \frac{4.5}{288.33} = 0.0156\text{s} \tag{18}$$

$\therefore$ Simulation delay time from joint 2 to end effector:

$$d_2 = \frac{0.0156}{0.0252} = 0.619\text{ss} \tag{19}$$

Similarly, delay times and simulation delay times for position sensor locations 5.0m from joint 1 (0.5m from joint 2) are; 0.01734s, 0.688ss (0.001734s, 0.0688ss).

4. SIMULATION RESULTS

Tracking results for a collocated sensor, a noncollocated sensor at the end effector and NMP correction are shown superposed in Fig. 5 (a) for IFDC and Fig. 5 (b) for FLSAC. Tracking starts at the lower left corner and proceeds clockwise. The IFDC strategy produces pronounced overshoots at each direction, whereas the FLSAC strategy improves tracking for both collocated and noncollocated sensors. The overshoot at the second (top right) direction in Fig. 5 (a) switch shows a distinct rightward shift attributable to the asynchronous control action in response to time-delayed end-effector positions. The remainder of the trajectory exhibits minimal difference between collocated, noncollocated (NMP) and NMP corrected case. Trajectories zoomed at the first (top left) direction switch of Figs. 5 (a) and (b) are presented in Figs. 6 (a) and (b) to show the differences between the three cases for IFDC and FLSAC strategies. The trajectory for the IFDC noncollocated (NMP) case has a greater amplitude than for the collocated case. But, the amplitude for the NMP corrected case is even greater thereby demonstrating a true representation of NMP response to control action.

In contrast, results shown in Fig. 5 (b) for the FLSAC strategy demonstrate minimal difference between noncollocated (NMP) and NMP corrected amplitudes but a large difference between them and the amplitude for the collocated case. However, the FLSAC strategy significantly reduces the amplitudes for all three cases. Hence, flexural vibrations are suppressed for greater tracking precision while stability is maintained.

Sensor locations on link 2 are modeled by different values of L_2 substituted into (8) and (9). For the sensor located 0.5m from the elbow joint a circular trajectory is obtained as shown in Figs. 7 (a) and (b). For IFDC the trajectory exhibits erratic vibratory tracking behavior shown in Fig. 7 (a), whereas FLSAC produces a smooth circular trajectory shown in Fig. 7 (b). The difference between noncollocated (NMP) and NMP corrected results is minimal for both control strategies. All trajectories shown in Figs. 5 (a), (b), 6 (a), (b) and 7 (a), (b) are stable. Results confirm the FLSAC strategy is effective in suppressing link vibration, provides enhanced tracking control and maintains stability for noncollocated sensors especially located at the end effector which is of primary interest. Hyperstability conditions are

circumvented. Simulation clock times are 1 min 17 sec for IFDC and 1 min 40 sec for FLSAC.

5. CONCLUSION

IFDC with NMP time-delay synchronized control action has a minimal effect in compensating for NMP response or reducing vibration amplitude. In contrast, FLSAC effectively suppresses link flexural vibrations and enhances tracking control with noncollocated sensors. Tracking stability is maintained while hyperstability constraints are circumvented.

REFERENCES

Green A. and J.Z. Sasiadek (2005a). Adaptive Control of a Flexible Robot Using Fuzzy Logic. *AIAA Journal of Guidance, Control and Dynamics*, **28**, 36-42.

Green A. and J.Z. Sasiadek (2005b). Sensor Location Effect on Flexible Robot Stability and Control. *Proceedings of the IFAC World Congress (Praha'05),* Elsevier, Oxford.

Stieber, M.E., G. Vukovich and E. Petriu (1997). Stability Aspects of Vision-Based Control for Space Robots. In: *Proceedings of the IEEE International Conference on Robotics and Automation*, IEEE Press, Piscataway, NJ, 2771-2776.

Liang, S-C and M.J. Balas (1990). Direct Model Reference Adaptive Control in Large Space Structures Using Hyperstability, *Proceedings of the IEEE International Conference on Systems Engineering*, IEEE Press, Piscataway, NJ, 70-76.

Karkoub, M., G.J. Balas and K. Tamma (1995). Colocated and Noncolocated Control Design via μ-Synthesis for Flexible Manipulators," *Proceedings of the American Control Conference*, Omnipress, Madison, WI, 3321-3325.

Ryu, J-H., D-S. Kwon and B. Hannaford (2004). Control of a Flexible Manipulator with Noncollocated Feedback: Time-Domain Passivity Approach. *IEEE Transactions on Robotics, Control and Dynamics*, **20**, 776-780.

Alexander H.L. (1988). Control of Articulated and Deformable Space Structures. In: *Machine Intelligence and Autonomy for Aerospace Systems*, (E. Heer and H. Lum, Ed), pp. 327-347, AIAA Progress in Astronautics and Aeronautics, AIAA, Washington, DC.

De Luca, A., and B. Siciliano (1991). Closed-form Dynamic Model of Planar Multilink Lightweight Robots. *IEEE Transactions on Systems, Man and Cybernetics*, **21**, 826-839.

Moallem, M., R.V. Patel and K. Khorasani (2000). Flexible-Link Robot Manipulators: Control Techniques and Structural Design. Lecture Notes in Control and Information Sciences, Vol. 257, Springer-Verlag, London.

Slotine J. –J. E. and W. Li (1991). *Applied Nonlinear Control*, Prentice-Hall, Upper Saddle River, NJ.

Thomson, W.T (1981). *Theory of Vibration with Applications*, (2nd Ed), Prentice-Hall, Upper Saddle River, NJ.

Matlab 6, Simulink 4 (2001). Control Systems and Fuzzy Logic Toolboxes, Release 12, The Mathworks, Inc., Natick, MA.

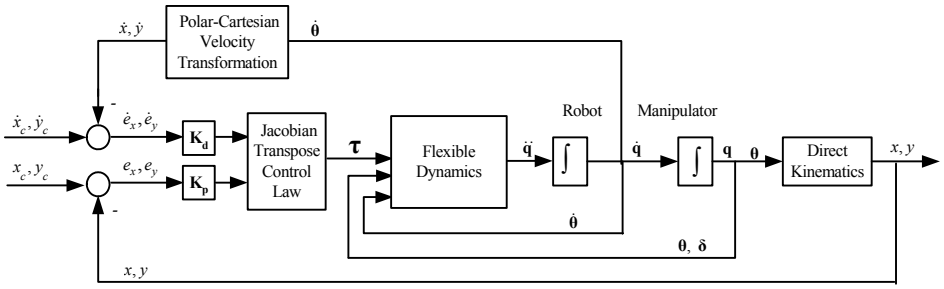

Fig. 3. IFDC strategy.

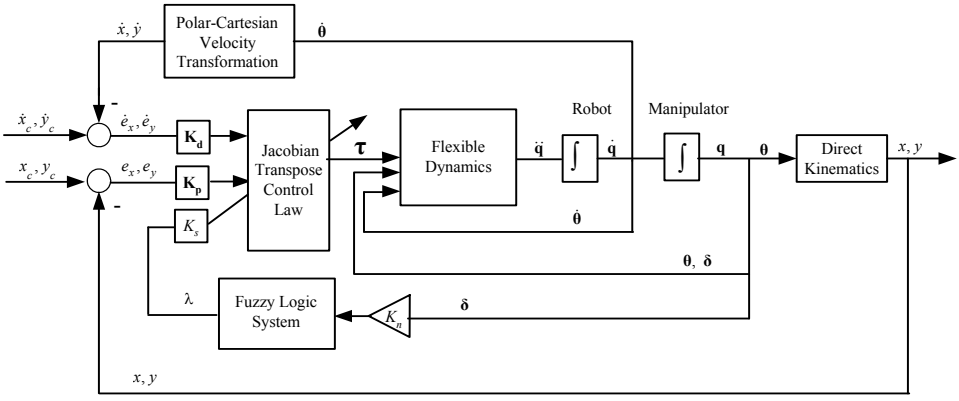

Fig. 4. FLSAC strategy.

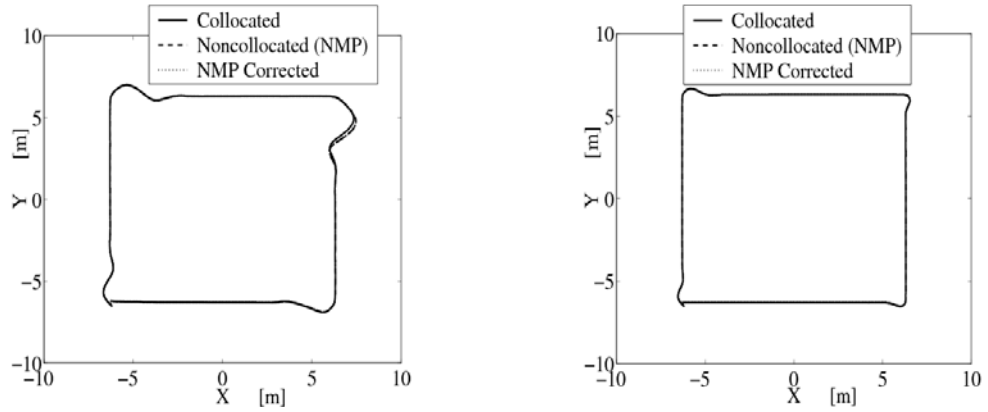

(a) (b)

Fig. 5. (a) IFDC with collocated sensor, sensor at end effector and NMP corrected, (b) FLSAC with collocated sensor, sensor at end effector and NMP corrected.

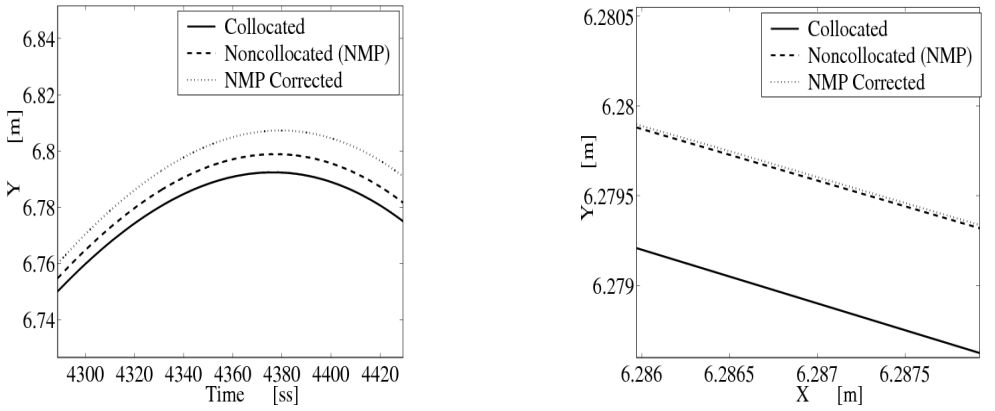

(a) (b)

Fig. 6. (a) IFDC with collocated sensor, sensor at end effector and NMP corrected (zoomed at first direction switch), (b) FLSAC with a collocated sensor, sensor at end effector and NMP corrected (zoomed at first direction switch).

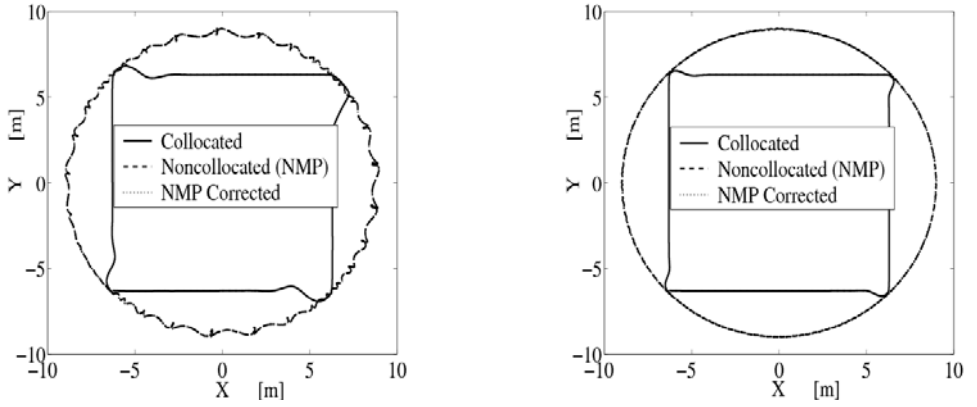

(a) (b)

Fig. 7. (a) IFDC with collocated sensor, sensor at 0.5m from elbow joint and NMP corrected, (b) FLSAC with a collocated sensor, sensor at 0.5m from elbow joint and NMP corrected.